A Snake-Inspired Multi-Segmented Magnetic Soft Robot Towards Medical Applications

Chen Wang, Venkata Rithwick Puranam, Sarthak Misra, *Senior Member, IEEE*, and Venkatasubramanian Kalpathy Venkiteswaran, *Member, IEEE*

***Abstract*—Magnetically-actuated soft robots have potential for medical application but require further innovation on functionality and biocompatibility. In this letter, a multi-segmented snake-inspired soft robot with dissolvable and biocompatible segments is designed. The actuation response under external magnetic field is investigated through simulations and experiments. A dissolve-controllable mixture of gelatin, glycerol and water (GGW) in a mass ratio of 1:5:6 is used to form the structure of the robot. The dissolution of GGW in water and mucus is tested. Magnetic cubes made of silicone rubber mixed with ferromagnetic particles are used to achieve snake-like motion under the influence of a rotating magnetic field. The motion of the robot is tested under different magnitudes and frequencies of the magnetic field. The ability of the robot to navigate obstacles, move over ground and under water as well as on the oil-coated surface, dissolve and release a drug is demonstrated through experiments. The combination of multi-segmented design and biocompatible and dissolvable materials illustrates the potential of such robots for medical applications.**

***Index Terms*—Soft robots, biodegradable materials, bioinspiration, magnetic actuation, medical robotics.**

I. Introduction

SOFT robots have strong potential for use in medical applications, particularly minimally invasive surgery (MIS), since their shape-programmable soft bodies are more flexible than their rigid counterparts in enclosed and confined spaces [1], [2]. Existing soft robots have been demonstrated to be maneuverable and controllable [3]. However, soft robots intended for MIS are required to be not only flexible, but also functional, bio-compatible and scalable to small sizes.

Manuscript received October 11, 2021; accepted March 4, 2022. Date of publication March 22, 2022; date of current version March 31, 2022. This letter was recommended for publication by Associate Editor E. W. Hawkes and Editor K. J. Cho upon evaluation of the reviewers' comments. This work was supported in part by the European Research Council (ERC) under the European Union's Horizon 2020 Research and Innovation Programme under Grant 866494 Project – MAESTRO and in part by the China Scholarship Council (CSC). *(Corresponding author: Venkatasubramanian Kalpathy Venkiteswaran.)*

Chen Wang is with the Surgical Robotics Laboratory, Department of Biomedical Engineering, University of Groningen and University Medical Centre Groningen, Groningen 9713, GZ, The Netherlands (e-mail: c.wang@umcg.nl).

Venkata Rithwick Puranam and Venkatasubramanian Kalpathy Venkiteswaran are with the Surgical Robotics Laboratory, Department of Biomechanical Engineering, University of Twente, Enschede 7500, AE, The Netherlands (e-mail: pvrithwick@gmail.com; v.kalpathyvenkiteswaran@utwente.nl).

Sarthak Misra is with the Surgical Robotics Laboratory, Department of Biomedical Engineering, University of Groningen and University Medical Centre Groningen, Groningen 9713, GZ, The Netherlands, and also with the Surgical Robotics Laboratory, Department of Biomechanical Engineering, University of Twente, Enschede 7500, AE, The Netherlands (e-mail: s.misra@utwente.nl).

Digital Object Identifier 10.1109/LRA.2022.3160753

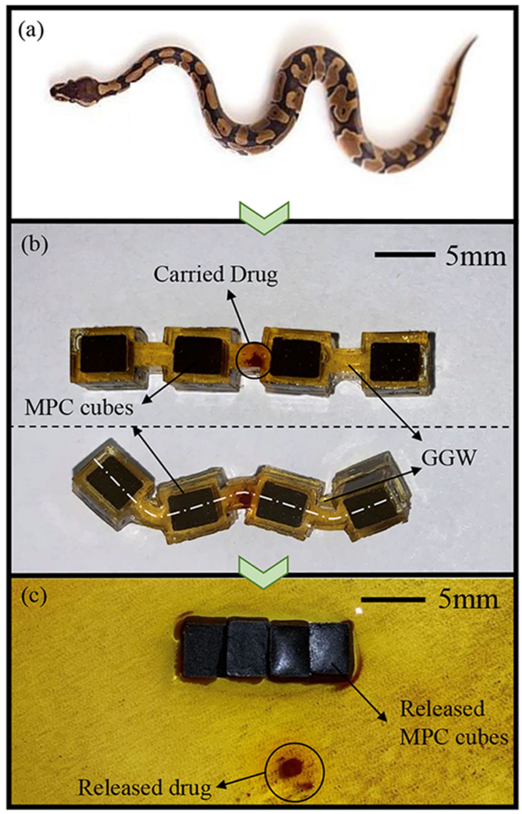

Fig. 1. (a) An example of biological snake locomotion with "S" shape is shown on the top (©Getty Images, courtesy of Ian Mcdonnell). (b) The soft robot inspired by the snake is shown on the middle, the centerline along each segment forms an "S" shape when the robot moves under an external magnetic field. The robot is made of magnetic polymer composite (MPC) and a biodegradable mixture of gelatin, glycerol and water (GGW). A mock-drug is carried in the middle link of the robot. (c) In warm water (40 °C), the GGW dissolves gradually, releasing the mock-drug and staining the water yellow. Once the GGW dissolves, the MPC cubes are attracted to each other and form a magnetic soft bar which can be moved using magnetic fields.

Multiple soft robots have been developed which were inspired by biological organisms such as caterpillar, worm, fish, and millipede [4]–[7]. Within these, snake-inspired soft robots have the capability to navigate narrow spaces due to the style of locomotion [8], [9]. Snake locomotion is generated through the propagation of sinusoidal waves along the backbone of the snake in the ground and vertical planes, which creates lateral undulation and shifting contact points with the ground [10], [11]. By exploiting this motion pattern, it is possible to create small

scale soft robots that can carry out functions in enclosed and confined spaces inside the human body such as gastrointestinal (GI) tract [1], [2], [12].

The flexibility and controllability of soft robots have been demonstrated through diverse actuation approaches. Electrical, pneumatic, acoustic, chemical and magnetic are currently the most widely used methods of actuation [3], [13]. In particular, magnetic actuation shows great promise for medical applications such as magnetic catheter ablation and electromagnetic navigation bronchoscopy, owing to its benefits including human-safe operation, wireless actuation and rapid response [14], [15]. Magnetic actuation eliminates the mechanical tether between robot and actuation unit. Untethered soft robots can navigate tortuous paths better than their tethered counterparts. Thus, magnetically-actuated soft robots can be used for MIS, targeted drug delivery and clinical diagnostics [1].

Many bio-inspired soft robots have been investigated within untethered magnetic devices. For instance, Joyee *et al.* analysed the motion mechanisms of the inchworm and designed a soft robot made of magnetic polymer composite (MPC) to mimic its motion [16]. Zheng *et al.* developed an ascidian-inspired soft robot that can crawl tumble, and pick and place objects [17]. Ren *et al.* demonstrated a sheet-shaped robot capable of multimodal locomotion to adapt to confined spaces [18]. Although these robots demonstrate flexibility, application requirements including the functionality and biocompatibility should be investigated.

Various efforts have been made to endow soft robots with practical functions for use in specific applications. Previously, a helical microrobot with a transport claw for drug delivery actuated using external magnetic field was proposed [19]. Venkiteswaran *et al.* showed legged robots with grippers, where motion and grasping can be controlled in tandem to grasp and release objects [20]. Additionally, origami-inspired magnetic soft materials such as magnetic responsive soft material (MRSM) film with reprogrammable magnetization patterns have been developed [21]. Moreover, chain-like soft devices have been studied as a promising approach for fabricating functional parts of soft robots with simple magnetic segments and soft links [22]. However, there are risks associated with losing track of the robots during operation and an inability to retrieve the robots after completing tasks when the robots are untethered, which poses problems for clinical applications if the robots are not biocompatible [23].

Biodegradable materials have been used to fabricate soft robots for safe operation inside the human body [24]. The functions of drug delivery and release of biodegradable materials have been demonstrated on microswimmers [25], [26]. There are several choices for biodegradable elastomers based on polyesters or hydrogels [27], [28]. A mixture of gelatin, glycerol and water (GGW) has been verified to be soft and biodissolvable, and the constituent components are commonly available [29].

In this paper, a snake-inspired magnetically-actuated soft robot with biocompatible and dissolvable components is designed, fabricated and tested (Fig. 1). The primary contribution of this study is the demonstration of multi-segment locomotion in combination with dissolvability and magnetic actuation, previously unseen in soft robots. The robot is able to move on ground, under water, on oil-coated surface and in a narrow tube. The motivation for this work is the improvement of functionality and biocompatibility for magnetic soft robots aimed at applications in the medical field. Multi-segmented soft robots have the potential to transport multiple components for group operation. Magnetic actuation enables untethered motion of the robot, while the use of biodegradable materials increases potential for medical application.

II. Design and Fabrication

In this section, the design of the multi-segmented magnetic soft robot is explained first. Then, the materials used for the robot are described. The dissolvability of the biodegradable mixture is tested. The fabrication process is also described in detail.

A. Design

The design of the multi-segmented magnetic soft robot is shown in Fig. 2(a). The robot body is made of four magnetic cubes joined through links made from the biodegradable mixture. The magnetic particles interact with an externally-generated magnetic field to produce magnetic torques which are used for motion actuation. The magnetic particles are mixed with silicone rubber which is biocompatible but undissolvable, thereby preventing the magnetic cubes from disintegrating. The biodegradable mixture is flexible, and the intermediate links twist and bend, enabling snake-like motion of the robot.

B. Materials

Two types of soft materials are used to fabricate the different parts of the robot. For magnetic actuation of the robot, a magnetic polymer composite (MPC) which comprises a silicone rubber matrix (Ecoflex-0010, Smooth-On Inc., USA) and a ferromagnetic powder of praseodymium-iron-boron (PrFeB) with a mean particle size of 5 μm (MQFP-16-7-11277, Magnequench GmbH, Germany) is selected. The mass ratio of the magnetic microparticles to the silicone rubber is 1:1 in this study. The MPC has mechanical properties such as relatively low elastic modulus (2 MPa) and high elongation at break (300%), endowing the robot with a soft internal structure. The elastic modulus of MPC used in the simulations is 75 kPa. Detailed mechanical properties as well as the characterization of MPC can be found in our previous work [7].

For the biodegradable part of the robot, a mixture of gelatin, glycerol, and water (GGW) with a mass ratio of 1:5:6 is used. This makes up the outer cover for the magnetic cubes and the links between the magnetic segments. The procedure of obtaining the biodegradable elastomer of GGW is as follows: gelatin is mixed with cold water first and allowed to bloom for 30 seconds. This is followed by adding glycerol and mixing them until the gelatin is thoroughly dispersed. The mixture is heated to 80 °C, and mixing is continued until the gelatin is sufficiently dissolved and the liquid is transparent. This liquid is then used to create the body of the robot.

Changing the ratio of the mixture changes the dissolvability as well as the mechanical properties of GGW. By adding glycerol, the cross-linking property of gelatin is diminished

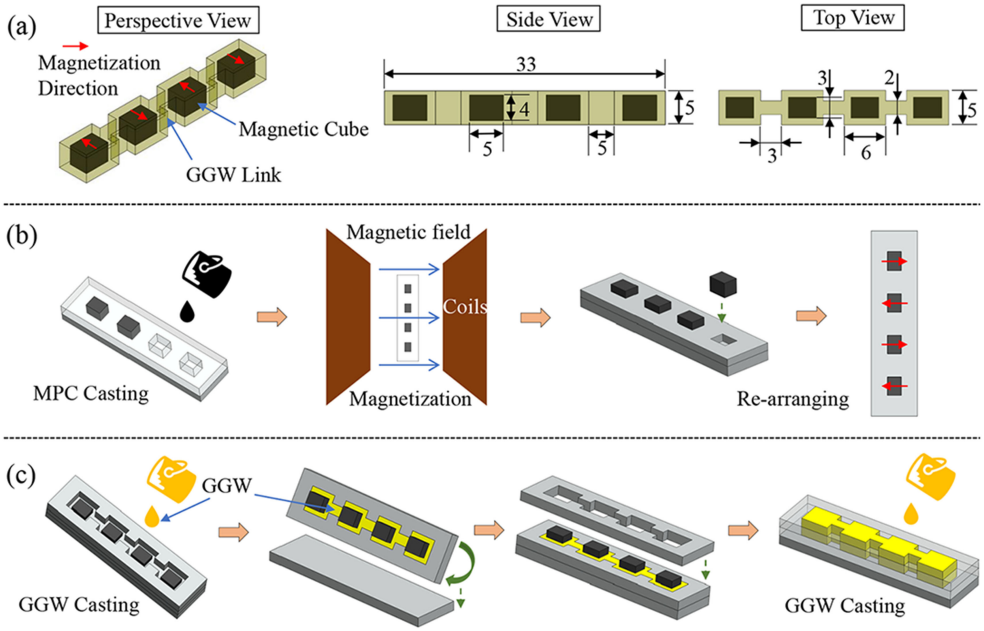

Fig. 2. Design and fabrication procedure of the soft robot. (a) The robot consists of inner magnetic cubes and outer biodegradable segments. The red arrows depict magnetic dipole directions. Dimensions are in mm and shown in the side and top views. (b) The casting and curing of magnetic polymer composite (MPC) are carried out first. The cubes are magnetized and rearranged in the second mold for casting the mixture of gelatin, glycerol and water (GGW). (c) GGW is then added in two layers to fully encapsulate the magnetic cubes and form the structure of the robot.

TABLE I
TIME FOR DISSOLUTION OF BIODEGRADABLE MIXTURE

Medium	Temperature	Ratio of Gelation : Glycerol : Water				
		1:1:6	1:3:6	1:5:6	1:7:6	1:9:6
Water	50°C	14.5s	16s	18s	19.5s	22s
	37°C	40s	58s	75s	95s	150s
Mucus	37°C	38s	59s	72s	100s	162s
Dry plate	37°C	96s	155s	>500s	>500s	>500s
	50°C	43s	67s	98s	125s	196s

which increases the solubility of the mixture. Based on this, an experiment is carried out to test the dissolvability of the GGW in order to control the dissolution time of the robot for potential use in different applications. Cubes ($5 \times 5 \times 5\,\mathrm{mm}$) with various ratio of GGW are made and immersed in water at different temperature. Aside from the mixture ratio, the dissolution of GGW is also influenced by the environment temperature. An experiment is carried out to test the dissolvability of the GGW on an open hot dry plate. Additionally, in order to simulate environment conditions in digestive system, the GGW cubes are immersed in 3% mucus solutions (mucin from porcine stomach, Sigma-Aldrich, USA) at 37 °C. The times for full dissolution of the cubes are listed in Table I. There is no significant difference (max. 8 s) between water and mucus with respect to the dissolution time, whereas the dissolution time of GGW on the open hot dry plate is much longer. This may be because the open hot plate did not provide even heating for the GGW cube. However the results still verify that the temperature dominates the dissolution of the GGW when the mixture ratio is constant. For applications which require relatively long time, the highest ratio of glycerol in the mixture can be an option. Also, the motion speed of the robot is adjustable. These can provide sufficient time for the robot to complete simple clinical tasks. Additionally, glycerol is a plasticizer, and therefore, a higher mass ratio of glycerol in the mixture leads to softer cured GGW. The ratio of 1:5:6 is selected for this study. The elastic modulus of GGW used in the simulations is 0.41 MPa [29]–[32].

C. Fabrication

The inner cubes are fabricated using MPC as shown in Fig. 2(b). Molds are created using laser-cut acrylic (Poly-methyl methacrylate) to create the shape of the cubes. The MPC is set to cure at room temperature (24 °C) for four hours, and the mixture is degassed before curing. Then the molds with cured MPC inside are subjected to a magnetic field of 1 T using a large electromagnet, to obtain the desired magnetization profile. The magnetized cubes are then transferred to another mold and rearranged with staggered magnetic dipole directions. The GGW is cured around the cubes in two layers, encapsulating one half of the cubes at a time as shown in Fig. 2(c). The robot is cured in a refrigerator at 8 °C. After this two-step process, the GGW encapsulates the cubes fully and also forms the links between them.

III. MOTION ANALYSIS

In this section, the magnetic actuation and motion of the robot are described. The actuation strategy for straight and turning motion and their dependence on the magnetization directions of the cubes are explained first. Based on a theoretical model, the magnetic moment as well as the deformation of the robot

under different directions of the magnetic field are calculated. The postures of the robot under specific directions of magnetic field are shown and compared with the experimental results in next section.

The actuation magnetic field is generated using a set of electromagnetic coils. It can be assumed that the contribution of the magnetic field gradient is negligible. Therefore, the actuation of the robot is achieved by using the magnetic torque ($\mathbf{T} \in \mathbb{R}^3$) as given by

$$\mathbf{T} = \mu \times \mathbf{B}$$

where $\mu \in \mathbb{R}^3$ is the magnetic dipole moment, $\mathbf{B} \in \mathbb{R}^3$ is the magnetic field.

To actuate the robot, a magnetic field is provided in the YZ plane rotating about X axis as shown in Fig. 3(a). The magnetic dipoles of the magnetized cubes tend to align with the direction of the magnetic field. Due to the opposite directions of the magnetic dipoles on adjacent cubes, the torques acting on the cubes tends to bend and twist the intermediate GGW links. This leads to the lift of one edge of a cube and anchoring of the opposite edge resulting in an "S" shape of the robot body in both the horizontal and vertical planes. At different orientations of the external magnetic field, the bending and twisting of the GGW links changes. The reaction force between the cube and the plate surface pushes the robot forward as the magnetic field rotates from 0° to 360° around the X-axis.

The steering of the robot is achieved using the following approach. Changing the tilt angle β between the plane of rotation of the magnetic field and YZ plane (shown in Fig. 3(b)), changes the axis of the magnetic torque. If β is changed in small increments, the robot tends to align with the plane of rotation of the magnetic field. The direction of turning (left or right) can be altered by reversing the direction of β.

In order to analyze the mechanism of motion, each link of the robot is modeled as a cantilever beam, and the cubes are considered rigid (shown in Fig. 3(c)). Based on theoretical analysis under quasi-static condition, there are two couples of bending and twisting moment acting on the four cubes of the robot. The bending and twisting moment diagrams are shown in Fig. 3(d). As shown in Fig. 3(e), there is a phase difference (90°) between bending moment and twisting moment.

Assuming small linear deflections of the links, the bending angle (θ_b) and twisting angle (θ_t) for each segment are respectively calculated as:

$$\theta_b = \frac{Tl}{EI_b}\cos\phi \qquad \theta_t = \frac{Tl}{GI_t}\sin\phi,$$

where l is the length of the GGW link between the segments, ϕ is the magnetic field angle, E is elastic modulus of the link, G is the shear modulus, I_b is the area moment of inertia, and I_t is polar moment of inertia of cross section.

Considering the robot as a rigid body, the deformation of the robot can be calculated by the following kinematics equations:

$$\mathbf{P}_1 = \begin{bmatrix} \cos\theta_b & -\sin\theta_b & 0 \\ \sin\theta_b & \cos\theta_b & 0 \\ 0 & 0 & 1 \end{bmatrix} \begin{bmatrix} 1 & 0 & 0 \\ 0 & \cos\theta_t & -\sin\theta_t \\ 0 & \sin\theta_t & \cos\theta_t \end{bmatrix} \mathbf{P}_0,$$

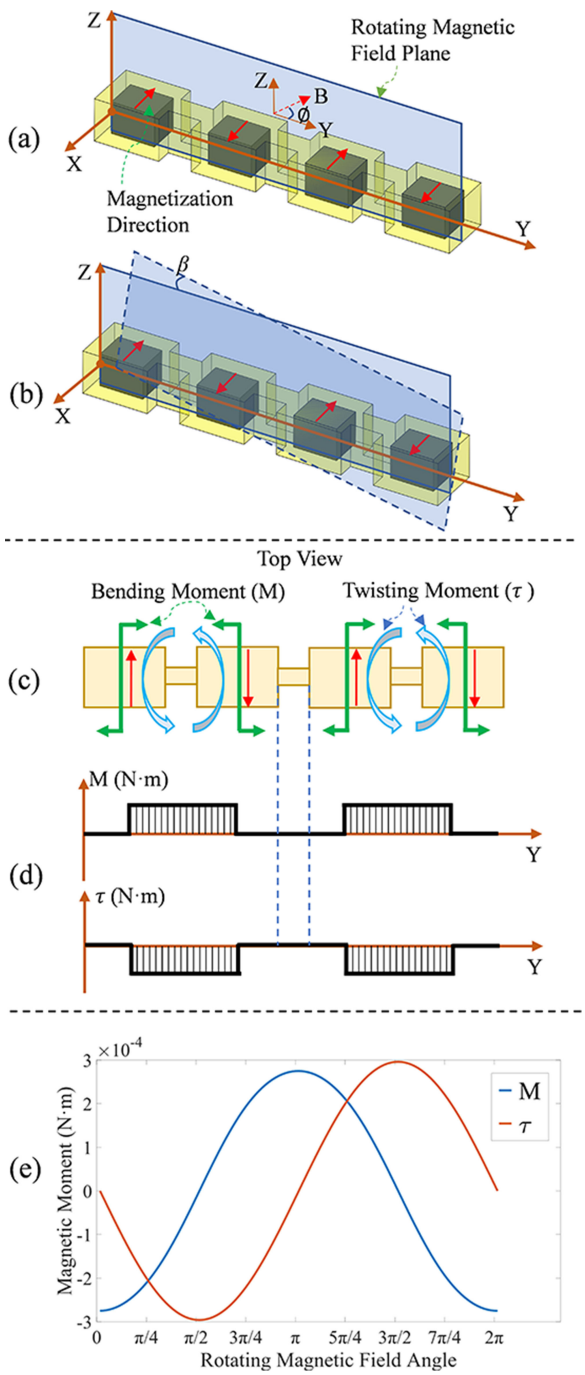

Fig. 3. Description of actuation methods and force analysis for the robot. (a) The robot moves forward as the magnetic field (B) rotates in the YZ-plane about the X-axis in the range $\phi \in [0°, 360°]$. (b) To steer the robot by turning left and right, the plane of rotating field is titled by the angle (β) to the YZ plane. (c) Two couples of bending and twisting moments act on the segments respectively. (d) The diagrams of bending and twisting show that the middle link is unstressed. (e) The phase difference between bending and twisting enable the robot to move.

where $\mathbf{P}_0$ represents the initial position of any selected point on the robot, $\mathbf{P}_1$ represents the new position of $\mathbf{P}_0$ after deformation. Based on the above equations, the simulations are carried out to describe the motion pattern of the robot using Matlab (2021a, Mathworks, USA). The vertices of each segment

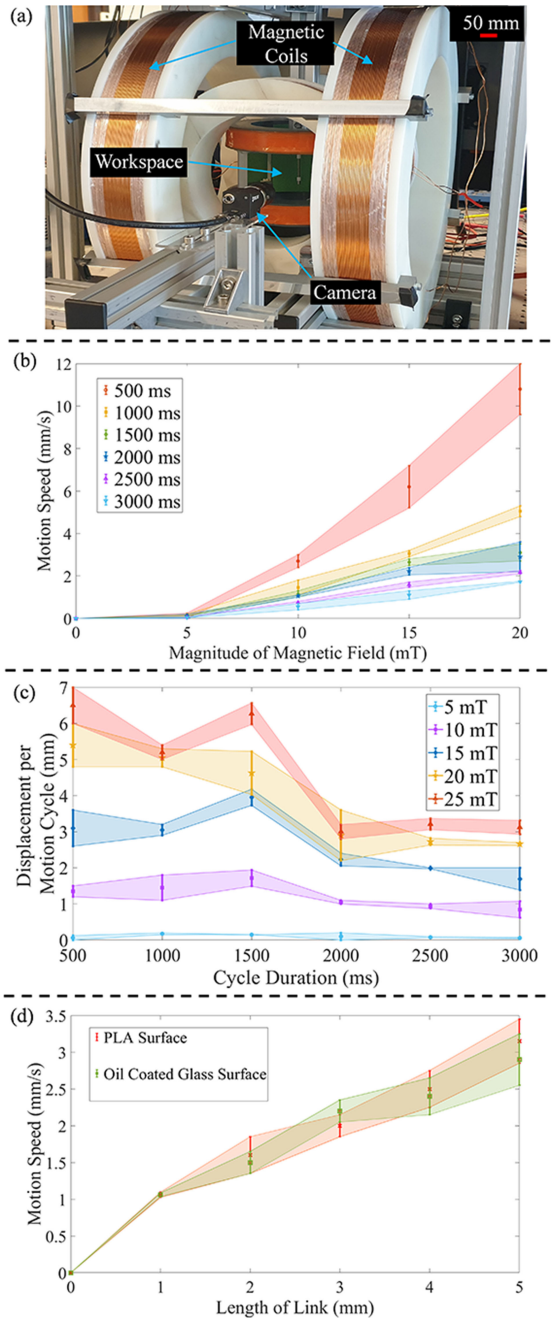

Fig. 4. (a) The setup for magnetic actuation. (b) Motion speed of the robot under different magnitudes and cycle duration of the magnetic field. (c) Displacement per actuation cycle under different cycle duration.(d) Motion speed of the robot with different link lengths at 15 mT magnitude and 1500 ms cycle duration of magnetic field.

and link are selected and used to draw out the contour of the robot. The friction between the robot and surface and the gravity of the robot are neglected in the simulation. A comparison of the theoretical predictions versus experimental results for the postures of the robot under different directions of the magnetic field is shown in Fig. 5.

IV. Experiments and Results

In this section, the experiments for demonstrating the motion and function of the robot are described, the results are used for verifying the simulation results as well. First, the experimental setup is introduced, followed by an experiment that shows the robot posture under changing orientation of the magnetic field. The motion speed under different cycle duration (frequency) and magnitudes of the magnetic field are tested. Experiments are carried out to demonstrate the maneuverability of the robot and the capability of moving on the low-friction oil-coated surface. In the final experiment, a robot carrying a mock-drug is controlled to move through a narrow opening, slither into a reservoir of water, dissolve and release the drug.

A. Experimental Setup

A setup consisting of six electromagnetic coils in a Helmholtz configuration with 12 × 12 × 12 cm workspace is used for magnetic actuation (see Fig. 4(a)). The setup can generate a uniform magnetic field up to 50 mT in any given direction. The surface of the setup for testing is 3D-printed Polylactic acid (PLA). A 3D printed box of 10 × 8 × 4 cm with obstacles and a water reservoir is used as the testbed for testing functionalities of the robot. Two cameras are used for observing and recording the top and side views of the experiments.

B. Robot Locomotion

The postures of the robot from both top view and side view under different directions of the magnetic field are shown in Fig. 5 (see supplementary video). Simulation results based on the analysis in Sec. III are shown in perspective view beside the experimental results. It is observed that pure bending occurs at 0° and 180°, pure twisting occurs at 90° and 270° respectively. In pure bending, the entire bottom face of the robot makes contact with the ground. In pure twisting and rest of the orientations, only one side edge of the first and last segment contacts with the ground. The two middle segments are always in face-to-face contact with the ground, serving to anchor the robot during motion.

The motion speed on PLA surface is tested and the results are shown in Fig. 4(b). The speed is influenced by both the time period of the actuation cycle and the strength of the magnetic field. Therefore, five groups of magnitude and six groups of cycle duration of the magnetic field are tested by controlling the variables. It is observed from the results that with a shorter cycle, the robot moves faster, and the robot moves slower when using a lower strength of magnetic field. The effect of actuation frequency on motion efficiency is tested by observing the relationship between cycle duration and displacement per motion cycle, shown in Fig. 4(c). In order to observe the influence of the link size on the robot locomotion, five robots with different link length (1–5 mm) and three robots with different link width (1–3 mm) are fabricated. The motion speed of each size of robot is tested under 15 mT and 1500 ms cycle duration. It is observed that robot motion speed increases with link length. The robot with low width (1 mm) on the link can be actuated under 5 mT, while the robot with wider link (3 mm) can be actuated under up to 50 mT. The robot with wider link is more stable at higher fields, whereas the thin link leads to robot rolling over. Moreover, the robot motion on the oil coated surface (1 mm thickness) coated surface is tested (see supplementary video). It can be seen from

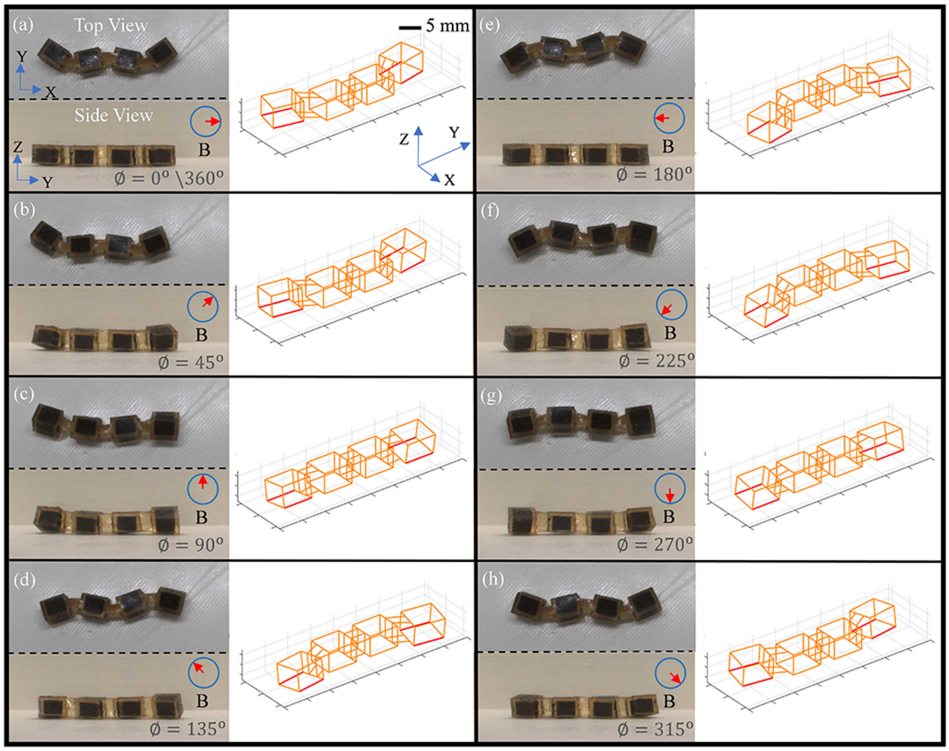

Fig. 5. Experimental and simulation results of postures of the robot under specific directions of magnetic field. Experimental results are shown in both top view and side view on the left; simulation result is shown in perspective view on the right. The magnitude of magnetic field is 15 mT. The orientation of the magnetic field is described using the angle ϕ (see supplementary video).

the results (Fig. 4(d)) that low-friction surface has little influence on robot locomotion. To study the repeatability, three identical robots are tested, and the mean error across the specimens is shown in the graphs.

C. Maneuverability

The robot can be controlled by changing the tilt angle β. An experiment is carried out to demonstrate the maneuverability of the robot (see supplementary video). A tube with 9 mm inner diameter and 12 mm outer diameter is prepared to mimic narrow spaces inside the body such as the small intestine. As shown in Fig. 6, the robot is controlled to turn by 90° and climb into the tube, and maneuver through the tube with bend of 90°.

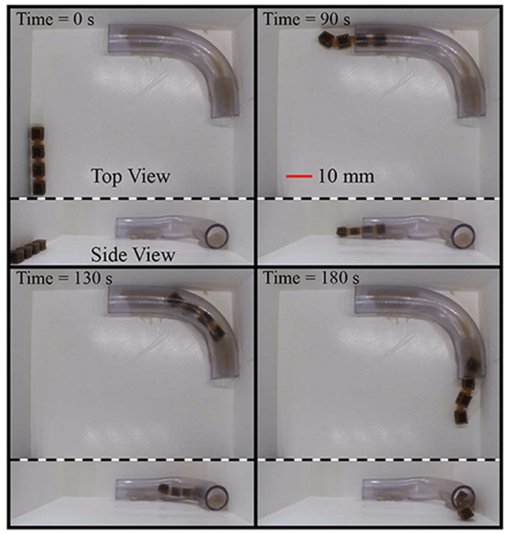

Fig. 6. Maneuverability test: the robot is steered to change orientation, climb into a tube of 9 mm inner diameter, maneuver through a 90° bend, and move out from the tube (see supplementary video).

D. Robot Functions

The functions of the robot demonstrated here are carrying a mock-drug, being steered to a target location in the workspace and drug release through dissolution (Fig. 7). The maneuverability of the robot is demonstrated by steering the robot to correct its heading and move through an obstacle (hole in the middle wall). After moving through the hole, the robot crawls down the slope into the reservoir of water. On the horizontal surface, a magnetic field of 10 mT is used, whereas on the slope a higher field of 15 mT is used.

In order to demonstrate the function of drug release, a small quantity of a mock-drug (Sudan Orange color dye, Merck, Germany) is integrated into the middle link. For higher contrast with the background, the robot is dyed orange by adding a small quantity of the dye to the GGW mixture. After the robot is steered through the obstacle, dissolution of the GGW outer links is achieved in warm water (40 °C). The robot is controlled to continuously rotate in the water in order to speed up the dissolution. The mock drug is released when the middle GGW link is dissolved, staining the water with the dye. After complete dissolution of the GGW, the four magnetic cubes attract each

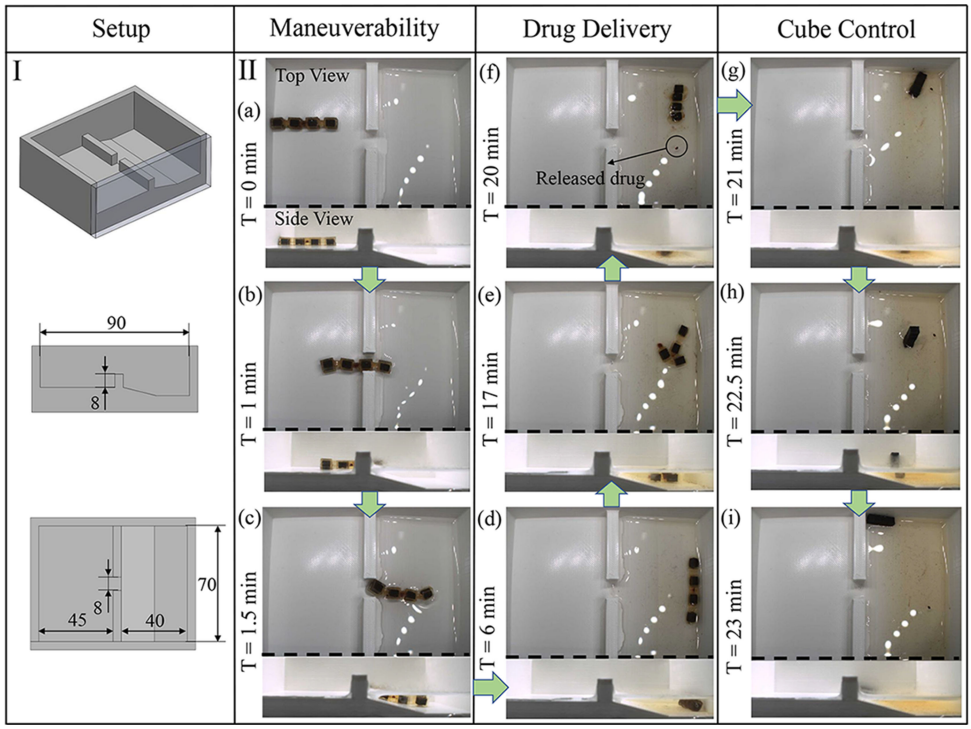

Fig. 7. Experiment to demonstrate robot drug delivery function I. Workspace for the experiment. Perspective, top and side view are shown. Dimensions are in mm. The angle of the slope is 30°. II. Experimental results. The maneuverability of the robot is demonstrated by steering through a hole in the wall (a, b, c). The robot enters the water, and rotates until the GGW links dissolve, releasing the mock-drug (d, e, f). After dissolution, the magnetic cubes are moved to one side of the workspace. T represents the experiment time (see supplementary video).

other and form a rectangular bar. Finally, the bar-shaped cube group is guided to one side of the workspace (See supplementary video).

E. Discussion

The experimental results support the predicted motion from simulations. By varying the magnitude and frequency of the external rotating magnetic field, the velocity of the multi-segment soft robot can be controlled. While the postures from the simulation and experiment appear similar, no quantitative comparisons are made in this study due to challenges in extracting 3D pose information from experiment videos. Fig. 4(b) shows increase in locomotion speed with the increase in magnetic field, which is expected since the magnetic torques increase, causing greater bending and twisting of the links. This holds up to 20 mT, above which the robot flips over due to high magnetic torque. From Fig. 4(c), it appears that the motion is more efficient at intermediate cycle durations, which may be due to a combination of factors affecting the dynamics of robot motion such as inertia and friction. Additionally, the motion velocity is related not only to the magnitude and frequency of the magnetic field but also the magnetization of the MPC cubes. Nevertheless, these aspects are not investigated in this study which aims to illustrate the robot motion as a proof-of-concept and demonstrate its functionality and biocompatibility.

It should be noted that slight deformation in the middle link is observed in the experimental results, while simulations predict no deformation. This could due to fabrication errors leading to imbalance of torques along the robot body (and subsequently displacement), and also by the friction between the robot and the ground, which is ignored in the simulation. However, the deformation of the middle link is sufficiently small that it can be used as a stable location for other functions, such as carrying camera or other tools.

For the drug delivery function demonstrated in this paper, the mock drug is only carried in the middle link. In fact, the volume of drug (or other reagents) carried by the robot can be increased by mixing them into the all the GGW parts. Thus the multi-segmented robot can carry a relatively large volume of drug ($520\,\mathrm{mm}^3$), compared to the single cube ($90\,\mathrm{mm}^3$).

For medical application in the future, further studies are required to enhance the biocompatibility of the robot. The composition of the PrFeB microparticles and the silicone rubber makes the current robot only partially biocompatible. There are several options that can make the robot fully biocompatible. First, ferromagnetic FePt nanoparticles have been shown to be noncytotoxic and biocompatible [33], which could be a replacement of the PrFeB used in this work. Second, coating with a layer of biocompatible materials can also make the magnetic particles or robots fully biocompatible. Additionally, the robot can be removed from the body after operation [5], [34], [35].

The robot can be miniaturized with the current fabrication methods (see supplementary video). The link of the miniaturized robot is made of silicon rubber, which connects the MPC cubes without an outer biodegradable layer. For further miniaturization, new biodegradable materials which suits micro- or milli- scale fabrication should be considered. Additionally, other technologies such as 3D printing and lithography can help to realize small-scale robot design.

V. Conclusion

In this paper, the locomotion and drug delivery function of a multi-segmented magnetic soft robot are demonstrated. The snake-like locomotion of the robot (previously not seen in magnetic soft robots) works on solid ground, in a narrow tube, on an oil-coated surface and also underwater. The drug delivery function is achieved by utilizing the GGW which is biodegradable. Although the MPC currently shows no toxicity, it can be made fully biocompatible. The mechanism of motion is analyzed through simulation and experiments. It has potential for optimization based on application requirements. Meanwhile, the dissolvability of the biodegradable GGW mixture in water suggests suitability for medical use. The combination of the snake-like locomotion and dissolvable materials endows the robot with the ability to transport multiple magnetic components and other payloads. Also, it is possible to control the magnetic components after dissolution, which is significant for robot retrieval.

This design has potential for further advancement, such as multi-modal locomotion of the robot including swimming in fluids. For use in the stomach or gastrointestinal tract, the stability of the locomotion should be investigated, since organs inside the body have uneven surfaces and are covered by body fluids such as mucus which provide lubrication. For further medical applications, miniaturization can be investigated. Also, sensor integration for tracking the robot inside the human body would be beneficial. The stable middle link of the robot provides a potential location for additional functions. Future work will focus on demonstrating improved clinical function of the robot in combination with closed-loop actuation and integrated sensing.

References

[1] M. Tonutti *et al.*, "The role of technology in minimally invasive surgery: State of the art, recent developments and future directions," *Postgraduate Med. J.*, vol. 93, no. 1097, pp. 159–167, 2017.

[2] M. Eshaghi *et al.*, "Design, manufacturing and applications of small-scale magnetic soft robots," *Extreme Mech. Lett.*, vol. 44, 2021, Art. no. 101268.

[3] D. Rus and M. T. Tolley, "Design, fabrication and control of soft robots," *Nature*, vol. 521, no. 7553, pp. 467–475, 2015.

[4] S. Kim *et al.*, "Soft robotics: A bioinspired evolution in robotics," *Trends Biotechnol.*, vol. 31, no. 5, pp. 287–294, 2013.

[5] W. Hu *et al.*, "Small-scale soft-bodied robot with multimodal locomotion," *Nature*, vol. 554, no. 7690, pp. 81–85, 2018.

[6] A. D. Marchese *et al.*, "Autonomous soft robotic fish capable of escape maneuvers using fluidic elastomer actuators," *Soft Robot.*, vol. 1, no. 1, pp. 75–87, 2014.

[7] V. K. Venkiteswaran *et al.*, "Bio-inspired terrestrial motion of magnetic soft millirobots," *IEEE Trans. Robot. Autom. Lett.*, vol. 4, no. 2, pp. 1753–1759, Apr. 2019.

[8] C. Branyan *et al.*, "Soft snake robots: Mechanical design and geometric gait implementation," in *Proc. IEEE/RSJ Int. Conf. Robot. Biomimetics*, 2017, pp. 282–289.

[9] C. D. Onal and D. Rus, "Autonomous undulatory serpentine locomotion utilizing body dynamics of a fluidic soft robot," *Bioinspiration Biomimetics*, vol. 8, no. 2, 2013, Art. no. 026003.

[10] A. A. Transeth *et al.*, "A survey on snake robot modeling and locomotion," *Robotica*, vol. 27, no. 7, pp. 999–1015, Dec. 2009.

[11] M. Mori and H. Hirose, "Locomotion of 3D snake-like robots-shifting and rolling control of active cord mechanism ACM-R3-," *J. Robot. Mechatronics*, vol. 18, no. 5, pp. 521–528, 2006.

[12] Y. Yang *et al.*, "Graphene-based light-driven soft robot with snake-inspired concertina and serpentine locomotion," *Adv. Mater. Technol.*, vol. 4, no. 1, 2019, Art. no. 1800366.

[13] V. Venkiteswaran and S. Misra, "Towards gradient-based actuation of magnetic soft robots using a six-coil electromagnetic system," in *Proc. IEEE/RSJ Int. Conf. Intell. Robots Syst.*, 2020, pp. 8633–8639.

[14] S. Ernst *et al.*, "Initial experience with remote catheter ablation using a novel magnetic navigation system: Magnetic remote catheter ablation," *Circulation*, vol. 109, no. 12, pp. 1472–1475, 2004.

[15] T. Gildea *et al.*, "Electromagnetic navigation diagnostic bronchoscopy: A prospective study," *Amer. J. Respir. Crit. Care Med.*, vol. 174, no. 9, pp. 982–989, 2006.

[16] E. B. Joyee and Y. Pan, "A fully three-dimensional printed inchworm-inspired soft robot with magnetic actuation," *Soft Robot.*, vol. 6, no. 3, pp. 333–345, 2019.

[17] S. Zheng *et al.*, "Ascidian-inspired soft robots that can crawl, tumble, and pick-and-place objects," *IEEE Trans. Robot. Autom. Lett.*, vol. 6, no. 2, pp. 1722–1728, Feb. 2021.

[18] Z. Ren *et al.*, "Soft-bodied adaptive multimodal locomotion strategies in fluid-filled confined spaces," *Sci. Adv.*, vol. 7, no. 27, 2021 Art. no. eabh2022.

[19] S. Tottori *et al.*, "Magnetic helical micromachines: Fabrication, controlled swimming, and cargo transport," *Adv. Mater.*, vol. 24, no. 6, pp. 811–816, 2012.

[20] V. K. Venkiteswaran *et al.*, "Tandem actuation of legged locomotion and grasping manipulation in soft robots using magnetic fields," *Extreme Mech. Lett.*, vol. 41, 2020, Art. no. 101023.

[21] H. Deng *et al.*, "Laser reprogramming magnetic anisotropy in soft composites for reconfigurable 3D shaping," *Nature Commun.*, vol. 11, no. 1, 2020, Art. no. 6325.

[22] J. Zhang *et al.*, "Voxelated three-dimensional miniature magnetic soft machines via multimaterial heterogeneous assembly," *Sci. Robot.*, vol. 6, no. 53, 2021, Art. no. eabf0112.

[23] M. Sitti *et al.*, "Biomedical applications of untethered mobile milli/microrobots," *Proc. IEEE Inst. Electr. Electron. Eng.*, vol. 103, no. 2, pp. 205–224, Feb, 2015.

[24] S. R. Goudu *et al.*, "Biodegradable untethered magnetic hydrogel milli-grippers," *Adv. Funct. Mater.*, vol. 30, no. 50, 2020, Art. no. 2004975.

[25] U. Bozuyuk *et al.*, "Light-triggered drug release from 3D-printed magnetic chitosan microswimmers," *ACS Nano*, vol. 12, no. 9, pp. 9617–9625, 2018.

[26] H. Ceylan *et al.*, "3D-printed biodegradable microswimmer for theranostic cargo delivery and release," *ACS Nano*, vol. 13, no. 3, pp. 3353–3362, 2019.

[27] M. Baumgartner *et al.*, "Resilient yet entirely degradable gelatin-based biogels for soft robots and electronics," *Nature Mater.*, vol. 19, no. 10, pp. 1102–1109, 2020.

[28] S. Miyashita *et al.*, "Ingestible, controllable, and degradable origami robot for patching stomach wounds," in *Proc. IEEE Int. Conf. Robot. Automat.*, 2016, pp. 909–916.

[29] J. Hughes and D. Rus, "Mechanically programmable, degradable & ingestible soft actuators," in *Proc. IEEE/RSJ Int. Conf. Soft Robot.*, 2020, pp. 836–843.

[30] M. Thomazine *et al.*, "Physical properties of gelatin films plasticized by blends of glycerol and sorbitol," *J. Food Sci.*, vol. 70, no. 3, pp. E172–E176, 2005.

[31] G. V. N. Rathna, "Gelatin hydrogels: Enhanced biocompatibility, drug release and cell viability," *J. Mater. Sci.*, vol. 19, no. 6, pp. 2351–2358, 2008.

[32] N. Suderman *et al.*, "The effect of plasticizers on the functional properties of biodegradable gelatin-based film: A review," *Food Biosci.*, vol. 24, pp. 111–119, 2018.

[33] V. Kadiri *et al.*, "Biocompatible magnetic micro- and nanodevices: Fabrication of fept nanopropellers and cell transfection," *Adv. Mater.*, vol. 32, no. 25, 2020, Art. no. 2001114.

[34] Y. Kim *et al.*, "Ferromagnetic soft continuum robots," *Sci. Robot.*, vol. 4, no. 33, 2019, Art. no. eaax7329.

[35] D. Son *et al.*, "Magnetically actuated soft capsule endoscope for fine-needle biopsy," *Soft Robot.*, vol. 7, no. 1, pp. 10–21, 2020.